Controlling electron transfer between the two cofactor chains of Photosystem I by the redox state of one of their components.

Stefano Santabarbara[†‡§], Bradford Bullock[¶], Fabrice Rappaport[‡*], Kevin Redding[†*]

[†]Department of Chemistry & Biochemistry, Arizona State University, 1711 S. Rural Rd., Tempe, Arizona 85287, U.S.A. [‡]Institut de Biologie Physico-Chimique, UMR7141 CNRS-UPMC, 13 Rue Pierre et Marie Curie, 75005, Paris, France [§]Istituto di Biofisica, Consiglio Nazionale delle Ricerche, Via Celoria 26, 20133 Milano, Italy. [¶]Dept. Chemistry, University of Alabama, 206 Shelby Hall, 250 Hackberry Lane, Tuscaloosa, AL 35487-0336

Supporting Material

i) Modeling of secondary electron transfer reactions in the RC of PSI

The kinetics of secondary electron transfer reactions reaction in PSI has been modeled, as previously described in detail (1, 2), by solving a system of linear differential equations that consider explicitly three states, PhQ_A^-, PhQ_B^- and F_X^-. The rate constant associated with each ET event was determined according to Marcus theory of electron transfer, in the "high-temperature approximation" that does not explicitly consider coupling with the nuclear modes (3–4):

$$k_{et} = \frac{2\pi}{\mathrm{h}} \frac{\left|H_{DA}\right|_0^2 e^{-\beta X_{DA}}}{\sqrt{4\pi\lambda_{tot} k_b T}} e^{-\frac{(\Delta G^0 + \lambda_{tot})^2}{4 k_b T \lambda_{tot}}} \qquad \text{Equation S1}$$

For the maximal value of the electron coupling factor, $\left|H_{DA}\right|_0^2$, we consider a value of ~1.5 x10^{-3} eV^2 (e.g. 5 – 6), attenuated exponentially by a factor β = 1.3 – 1.4 $Å^{-1}$ (7, 8) weighted for donor-acceptor distance X_{DA}, taken from the PSI structure from *T. elongatus* (9, PDB ID: 1JB0). The remaining parameters in the simulations are the (total) reorganization energy (λ_{tot}) and the standard Gibbs free energy difference ΔG^0. In order to limit the number of variables, the value of λ_{tot} has been

initially taken to be equal for all the reactions considered (λ_{tot}=0.7 eV). This value lies in the middle of the reported spread for ET within proteins (7, 8), and is similar to values obtained from the analysis of experimental data (10 – 12) and kinetic modeling (1, 2) of PhQ^- oxidation reactions. Therefore, only the ΔG^0 values need to be adjusted to describe qualitatively the experimental results. Since the model considers explicitly three states, the decay is described by three exponential lifetimes (and three associated amplitudes). Two of the lifetimes fall in the 5–30 ns interval and are considered to describe collectively the fastest phase of PhQ^- oxidation, whereas the remaining one describes the slowest phase observed experimentally (1, 2).

As previously discussed (1, 2, 13, 14), it is possible to obtain a good *qualitative* agreement between the experimental results and the simulations considering that $\Delta G^0_{PhQ_A^- \rightarrow F_X} > 0$ and $\Delta G^0_{PhQ_B^- \rightarrow F_X} < 0$, (i.e., oxidation of PhQ_A^- is slightly endergonic, with a value of ~1–2 k_bT). Although the numerous approximations implicitly made in the model prevent going beyond a qualitative description of the ET kinetics, it has yielded a rather good agreement between simulated and experimental lifetimes and amplitudes of the slow and fast PhQ^- oxidation phases (1, 2, 13, 14). The most relevant parameters to model the wild-type kinetics are reported in Table S1.

In order to simulate the kinetics in PsaA-F689N with minimal perturbation of the WT parameters, the midpoint potential of the PhQ_A/PhQ_A^- couple needs to be downshifted by 125 mV (thereby $\Delta G^0_{PhQ_A^- \rightarrow F_X}$ = 135 meV ~ $5\,k_bT$), so that this reaction is rather unfavorable, even when coupled with the very favorable oxidation of F_X^- ($\Delta G^0_{F_X^- \rightarrow F_{A/B}}$ < –150 meV). This yields a relatively good description of the lifetimes measured experimentally, including the extremely slow 17-μs component, as well as the faster decay of the rapid PhQ^- oxidation phase (Table S1). However, the amplitude associated with the slow 17-μs component is predicted by the simulation to be significantly larger than was seen experimentally (Fig. S1 and Table S1). A possible explanation for this discrepancy is that the mutation changes parameters besides the midpoint potential of PhQ_A/PhQ_A^-, such as modification of the reorganization energy (λ_{tot}) or the nuclear mode coupled to the ET reactions ($\bar{\omega}$).

This would not be unprecedented, since it was necessary to consider changes both in ΔG^0 as well as in $\bar{\omega}$ to explain the temperature-dependence of the kinetics in the PsaA-L722T mutant of *C. reinhardtii* (15). As the nuclear modes are not treated explicitly, due to the high-temperature approximation in our model, we altered the value of λ_{tot} to obtain a closer match between the simulations and experimental results. Raising the value of $\lambda_{tot,\mathrm{PhQ_A^-}\rightarrow\mathrm{F_X}}$ from 0.7 to 1 eV and that of $\Delta G^0_{\mathrm{PhQ_A^-}\rightarrow\mathrm{F_X}}$ from 10 meV to 115 meV in PsaA-F689N yields lifetimes that match experimental values well (Table S1). Importantly, the amplitude ratio of the slow:fast PhQ^- phases is now predicted to be ~0.80:0.20 in the mutant, which agrees well with the value estimated from the data (0.75:0.25, averaged over the near-UV PhQ^- absorption band).

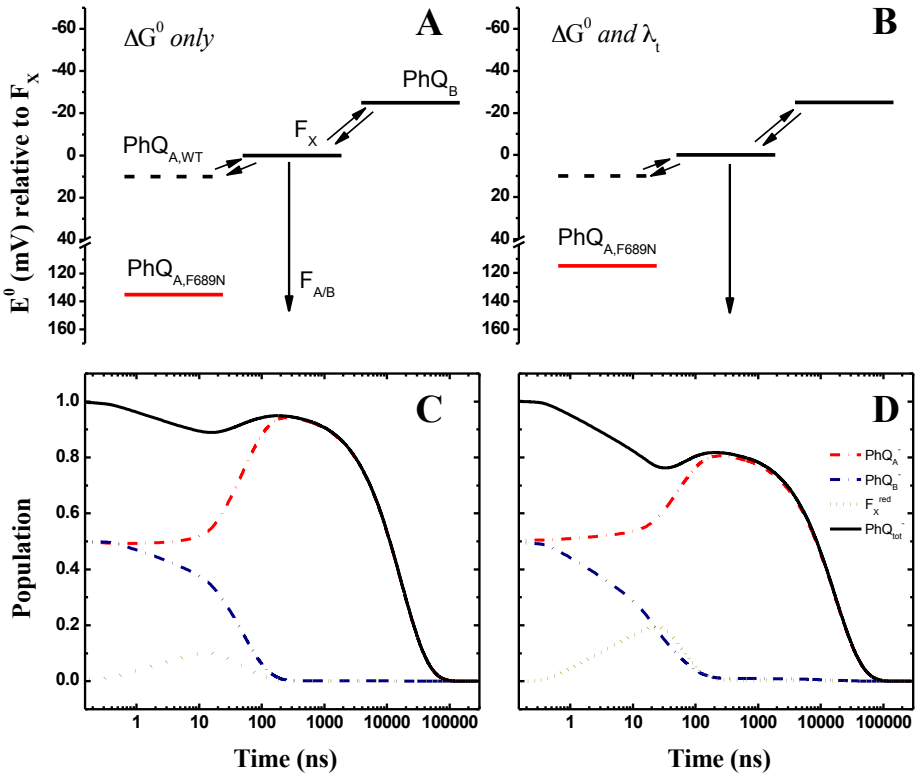

Figure S1. Simulations of ET kinetics in the PsaA-F689N mutant: energetics of the system (**A, B**) and calculated population evolutions (**C, D**). **Panels A** and **C** depict the situation obtained when modifying *only* the redox potential of $\mathrm{PhQ_A}/\mathrm{PhQ_A^-}$, and hence the free energy difference for the oxidation reaction in the mutant with respect to the wild type. **Panels B** and **D** display the simulation with alterations of both the standard free energy change and the reorganization energy of $\mathrm{PhQ_A^-}$ oxidation. Population evolution of $\mathrm{PhQ_A^-}$ (red dash-dotted lines), $\mathrm{PhQ_B^-}$ (blue dash-dotted lines) and $\mathrm{F_X}$

(golden dotted lines) derived from the modeling are shown. The solid black line depicts the "total" population evolution of PhQ^- (i.e., $PhQ_A^- + PhQ_B^-$).

Table S1. Values of the parameters used to simulate ET reactions in PS I.

	Input Parameters			Simulation Outputs				
	ΔG^0 (meV)	λ_{tot} (meV)	k_i^{-1} (ns)	τ_i (ns)	$A_{i,\,PhQ_A}$	$A_{i,\,PhQ_B}$	$A_{i,\,F_X}$	$A_{i,\,PhQ_{A+B}}$
Wild Type								
$PhQ_A^- \rightarrow F_X$	+10	700	33	9.2	0.21	0.18	-0.44	0.39
$PhQ_B^- \rightarrow F_X$	-25	700	18	23.1	-0.27	0.19	0.12	-0.09
				261.5	0.56	0.13	0.32	0.70
PsaA-F689N								
$PhQ_A^- \rightarrow F_X$	+135	700	993	4.2	0.13	0.02	-0.15	0.15
$PhQ_B^- \rightarrow F_X$	-25	700	18	48.0	-0.59	0.48	0.15	-0.11
				17000	0.96	0.002	0.005	0.96
$PhQ_A^- \rightarrow F_X$	+115	1000	6130	11	0.095	0.25	-0.41	0.35
$PhQ_B^- \rightarrow F_X$	-25	700	18	48	-0.41	0.24	0.40	-0.16
				17000	0.82	0.01	0.004	0.81

Parameters used to simulate PhQ^- oxidation in WT and the PsaA-F689N mutants of *C. reinhardtii* and results of the simulations in terms of lifetimes (τ_i) and amplitudes (A_i). $A_{i,\,PhQ_{A+B}} \equiv A_{i,\,PhQ_A} + A_{i,\,PhQ_B}$ for each τ_i. Simulations were performed altering either only the value of $\Delta G^0_{PhQ_A^- \rightarrow F_X}$ or both $\Delta G^0_{PhQ_A^- \rightarrow F_X}$ and $\lambda_{tot,PhQ_A^- \rightarrow F_X}$. The parameters used to model the oxidation of reduced F_X were held fixed for all simulations and corresponded to $\Delta G^0_{F_X^r \rightarrow F_A}$ = -155 meV and $\lambda_{tot,F_X^r \rightarrow F_A}$ = 700 meV. The temperature in all simulations was 298 K. Initial conditions were: $PhQ_A^- = PhQ_B^- = 0.5;\ F_X = 0$.

ii) Analysis of pump-pump-probe kinetics.

Figure S2 shows a comparison of the pump-probe and the pump-pump probe kinetics at 445 nm. This wavelength was selected as a marker for $[P_{700}^{+}A_0^{-}]$ charge recombination, since the bleaching due to A_0^{-} is still significant at this wavelength, while the contributions of P_{700}^{+} and electrochromic shifts of nearby pigments are much less significant (16–18). The comparison of these two experiments shows negligible differences for the WT on the short time scale (<200 ns, when charge recombination is expected to occur (16–18)), whereas some difference occurs on the longer time scale dominated by P_{700}^{+} reduction. This is due to the fact that there is less pre-bound plastocyanin available after the second flash, when it is close to the first flash, causing the reduction of P_{700}^{+} to be overall slower (i.e., there is a shift in the amplitudes of the ~6-μs and ~60-μs components towards the latter). A similar difference in the long time scale is observed for the PsaA-F689N mutant. In addition, a slight difference is observed on the short time scale, the relative magnitude of which is comparable to that observed at 395 nm (see Figure 3B of the main body). However, it is much smaller, since the absorption difference at 445 nm is much smaller than at 395 nm in the $[PhQ^{-} - PhQ]$ difference spectrum (see Figure 2 of the main body).

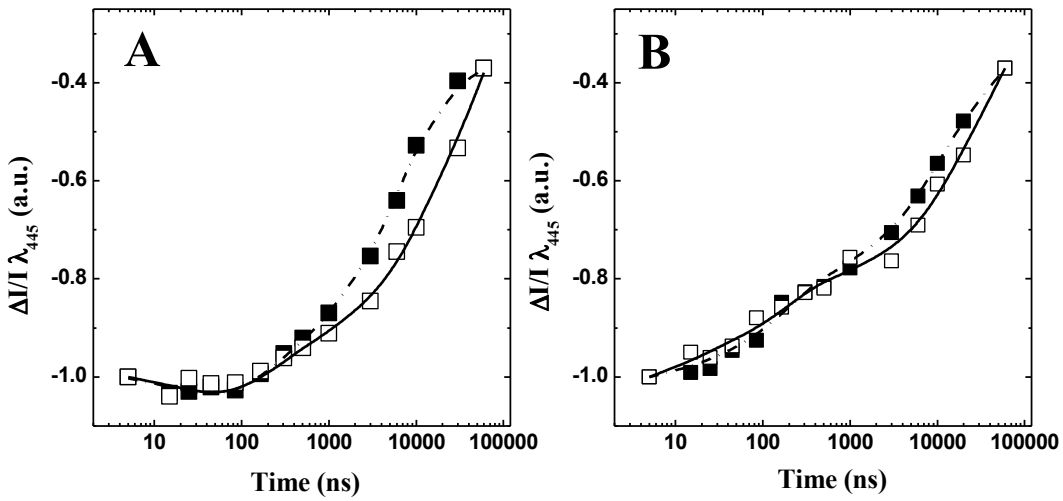

Figure S2. Comparison of kinetics monitored at 455 nm by pump-probe and pump-pump-probe (ΔT=15 μs) experiments in the WT (**A**) and the PsaA-F689N (**B**) strains. The open symbols and solid lines are the experimental data and fits of pump-pump-probe experiments, respectively, whereas the closed symbols and the dashed lines are the pump-probe kinetics acquired on the same sample using the pump-pump-probe set-up with the first pump pulse shuttered.

iii) Simulations of pump-pump-probe experiments

In the pump-pump-probe experiment reported in this study, the first pump pulse "prepares" the system in a given redox state of the cofactors in the reaction center. PSI can be present in four distinct "redox states" at the moment the second pump pulse is delivered to the sample at given delay time (ΔT) after the first actinic flash. Those are denoted as i) $\sigma_{P_{700}^{+}PhQ^{-}}$, the fraction in which the primary donor (P_{700}) is oxidized and the secondary acceptor (PhQ_A) is reduced; ii) $\sigma_{P_{700}^{+}PhQ^{-}}$ the fraction in which both P_{700} and PhQ_A are oxidized; iii) $\sigma_{P_{700}PhQ}$, the fraction in which P_{700} is reduced and PhQ_A is oxidized; iv) $\sigma_{P_{700}PhQ^{-}}$ the fraction in which both P_{700} and PhQ_A are reduced. The fractional populations of these four redox states, at any pump-pump delay ΔT, is the combinatorial probability of the normalized population evolution of $P_{700}^{(+)}$ and $PhQ_A^{(-)}$ that are determined from the classic pump-probe experiment. Figure S3 shows the calculated populations of the four different redox states, as a function of ΔT, for the wild-type and the PsaA-F689N mutant scenarios.

We now turn to consider how each of these redox states of the RC would evolve following the second actinic excitation in the pump-pump-probe experiment. We make the simple assumption that when the electron donor is oxidized (i.e. P_{700}^{+}) the system cannot undergo charge separation (i.e. it is "closed"). Therefore, fractions $\sigma_{P_{700}^{+}PhQ^{-}}$ and $\sigma_{P_{700}^{+}PhQ}$ would not contribute to the light-induced signal. We note that P_{700} may not be the primary electron donor (1, 19–21), and that initial charge separated state might be $[ec2_A^{+}ec3_A^{-}]$ instead. While the latter could be populated even in the presence of P_{700}^{+}, it has been shown in this case that charge recombination of the initial radical pair takes place in the sub-ns time range (22) and would therefore not contribute to the monitored transient absorption in our experiment. Therefore, the second pump pulse is assumed to be ineffective in PSI with P_{700}^{+}.

In the $\sigma_{P_{700}PhQ}$ fraction of centers, the system is simply reset and the evolution of the state produced by second pump flash should be the same as with a single flash. We can model this with by assuming that PSI RCs in this fraction will behave identically to those in the simple pump-probe experiment.

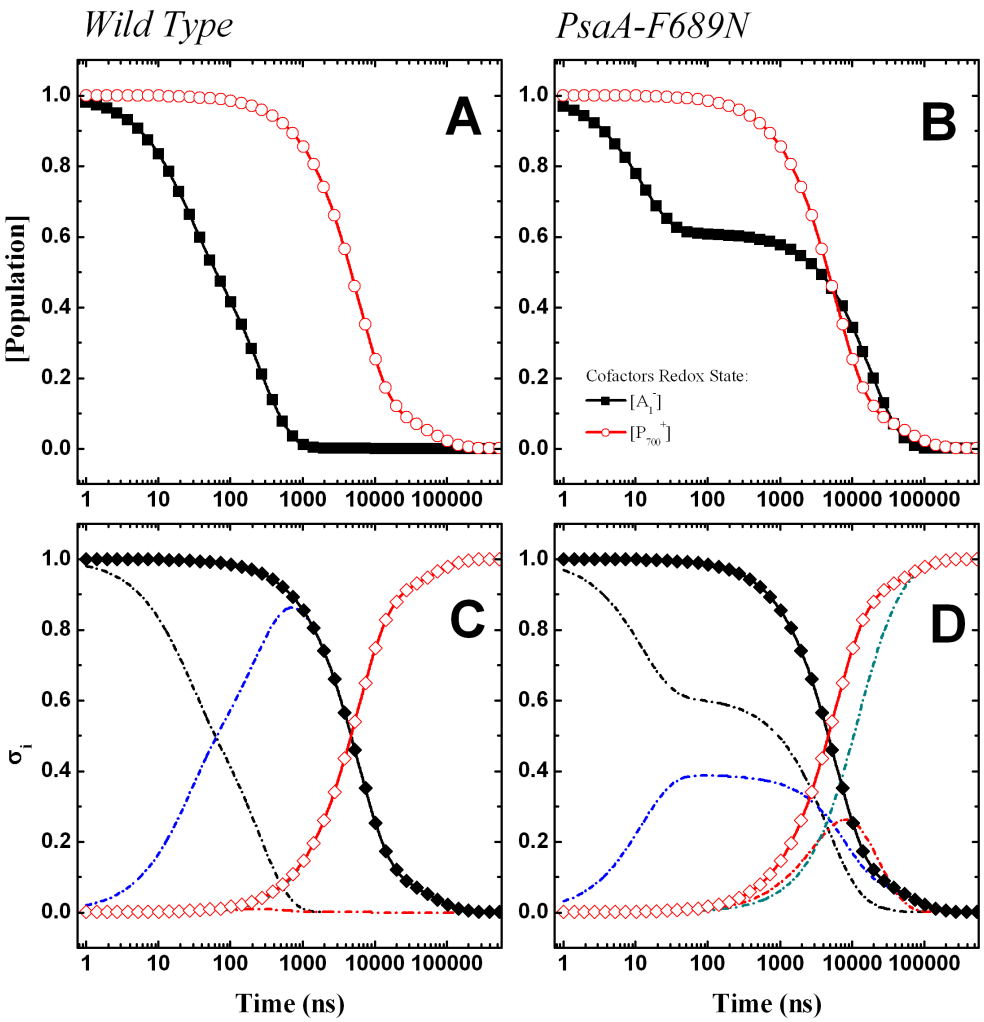

Figure S3. Comparison of the population evolution of P_{700}^{+} (open red symbols) and PhQ^{-} (solid black symbols) derived from the fits of the experimental data for the wild type (**A**) and the PsaA-F689N mutant (**B**). Note that both the "fast" and "slow" phases of P_{700}^{+} reduction and of PhQ^{-} oxidation have been included in the calculation. Probabilities of the different "redox states" of the system $\sigma_{P_{700}^{+/0}PhQ^{-/0}}$ calculated from the population evolution of the wild type (**C**) and the PsaA-F689N mutant (**D**): $\sigma_{P_{700}^{+}PhQ^{-}}$: dash-dotted black lines, $\sigma_{P_{700}^{+}PhQ}$: dash-dotted blue lines, $\sigma_{P_{700}PhQ^{-}}$: dash-dotted red lines, $\sigma_{P_{700}PhQ}$: dash-dotted green lines (not discernable in WT due to overlap with red line). Also shown are probabilities of PSI centers being "closed" ($\sigma_{closed} = \sigma_{P_{700}^{+}PhQ} + \sigma_{P_{700}^{+}PhQ^{-}}$: solid black diamonds) or "open" ($\sigma_{open} = \sigma_{P_{700}PhQ} + \sigma_{P_{700}PhQ^{-}}$: open red diamond).

The most interesting case is when both the electron donor and electron acceptor are reduced ($\sigma_{P_{700}PhQ^{-}}$). Under these conditions charge separation is initiated

in the presence of a charged molecule (PhQ_A^-) in close proximity to one of the cofactors involved in charge separation and this may have several consequences:

i) It may accelerate charge recombination of the initial radical pair formed after the second flash, thereby decreasing the overall yield of "long lived" P_{700}^+ (i.e., >5 ns, and thus detectable by our set-up).

ii) A second light-induced electron transfer in ETC_A may lead to the double reduction of PhQ_A. Because the quinol is stable and unavailable as an electron acceptor, its presence would promote $P_{700}^+ec3_A^-$ charge recombination. The signature of such a process would also be a decrease of long-lived P_{700}^+, as previously shown for a mutation in the PhQ biosynthetic pathway that leads to substitution of PhQ by plastoquinone in PSI; reduction of the introduced quinone to a quinol resulted in the decay of P_{700}^+ in the tens of ns (**23, 24**).

iii) The presence of PhQ_A^- may modify the energetics of charge separation in ETC_A by Coulombic interaction, making it more likely for charge separation to occur in ETC_B.

Based on these considerations, it is possible to describe the kinetics observed in pump-pump-probe experiments by the combination of three exponential decay functions $f^{pp}(t,\lambda) = \sum_{u=1}^{3} f_u^{pp}(t,\lambda)$ where:

$$f_1^{pp}(t,\lambda) = (\sigma_{P_{700}^+PhQ^-} + \sigma_{P_{700}^+PhQ}) \cdot (\sum_{i=1}^{n} A_i(\lambda) \cdot e^{-(\frac{t+\Delta t}{\tau_i})} + A_\infty(\lambda))$$

$$f_2^{pp}(t,\lambda) = (\sigma_{P_{700}PhQ}) \cdot (\sum_{i=1}^{n} A_i(\lambda) \cdot e^{-(\frac{t}{\tau_i})} + A_\infty(\lambda)) \qquad \text{Equation S2.}$$

$$f_3^{pp}(t,\lambda) = (\sigma_{P_{700}PhQ^-}) \cdot (\sum_{j=1}^{n} A_j(\lambda) \cdot e^{-(\frac{t}{\tau_j})} + A_\infty(\lambda))$$

As shown in Figure S3, the fraction of center $\sigma_{P_{700}PhQ^-}$ is significant only in the PsaA-F689N mutant. Hence, in the wild-type, the pump-pump-probe experiment only depends on $f_1^{pp} + f_2^{pp}$ (as described in Equation S2), so that the experimental results

can be described from the results of the standard pump-probe experiments alone. We note that, as shown in Figure 1, a residual difference absorption signal is observed at delay times longer than 100 μs. This is due to several processes occurring in the thylakoid membranes of whole *C. reinhardtii* cells (*e.g.* transmembrane electric field decay, cytochrome *f* redox changes). These processes, however, take place much later than ET events within the reaction centers and they are thus treated as a non-decaying component in the data fit (see Figure 1 of the main body). As a starting point, we assumed that the relative amplitude of the non-decaying fraction would scale linearly with the fraction of photochemically active PSI RCs. The simulations made according to this model, taking the parameters from the fits of the pump-probe experiment, are shown in Figure S4. The pump-pump-probe kinetics is described adequately for the sub-μs decay window by this model. However, the simulations failed to describe precisely the P_{700}^{+} reduction contribution. By allowing the amplitude of these "late" phases associated with P_{700}^{+} reduction to vary (without changing the lifetimes or amplitudes associated with PhQ^{-} oxidation), the agreement became excellent (Fig. S4). Changes in the decays in the μs time window are likely associated with a shift in the ratios of bound/unbound and/or oxidized/reduced plastocyanin at the time the second excitation pulse hits the RC. Since the relative amplitudes of the "fast" (~6 μs) and "slow" (~56 μs) reduction phases of P_{700}^{+} are related to the formation of the PSI-plastocyanin binary complex, and the slow phase, which is limited by dissociation/association of plastocyanin (e.g. **25, 26**), is comparable to the values of ΔT used in this study, a redistribution of the P_{700}^{+} reduction phases is expected. The simulations also show the relative contributions of signal arising from different initial redox states at ΔT, where it can be appreciated that the dominant contribution in the WT is $\sigma_{P_{700}PhQ}$ (dashed blue line) and that $\sigma_{P_{700}PhQ^{-}}$ (dashed magenta line) is completely negligible.

In contrast, the $\sigma_{P_{700}PhQ^{-}}$ fraction becomes significant in PsaA-F689N (Fig. S3). One of the possible scenarios when charge separation takes place in the presence of PhQ_A^{-} is that it is biased to occur preferentially on ETC_B, due to inhibition of primary radical pair formation, as the electron acceptor is located next to the PhQ_A^{-} anion. The simplest case that one can consider is that, in the presence of PhQ_A^{-}

i) no charge recombination occurs on ETC_A;

ii) no charge separation occurs down ETC_A and the electrons are all redirected down ETC_B; and

iii) the rates of the electron transfer reactions down ETC_B are unaffected by the presence of PhQ_A^-.

Point (iii) is an approximation because the kinetics of PhQ_B^- oxidation may be influenced by the presence of PhQ_A^- and F_X^- (see section 1 of the Supplementary material). However, since the dominating lifetime describing PhQ_B^- approaches the value of the inverse of kinetic rate constant associated to the $PhQ_B^- \rightarrow F_X$ event, this approximation appears to be reasonable, especially since the simulations are meant to provide only a semi-qualitative description of the pump-pump-probe experiments.

The results of the simulation made under these assumptions are also shown in Figure S4. It can be seen that they nicely fit the experimental results, but for a slight difference in offset that, when allowed to change freely, yields a very satisfactory description of the data. As in the case of the WT, the change in offset is likely due to changes in the fast:slow P_{700}^+ reduction phases by plastocyanin, which in the PsaA-F689N mutant strain are partially overlapped by the 17-µs PhQ^- oxidation component and are therefore less obvious. This bears little consequence for the interpretation of the transient absorption in the sub-µs time window, which is the central issue dealt with in this study.

One of the critical advantages of these simulations is that it allows one to discriminate the contributions of the different populations to the decay observed after the second excitation (Fig. S4 panels B and D). In the WT, the contribution of $\sigma_{P_{700}PhQ^-}$ is essentially nonexistent, and the closed fractions cause an offset. Thus all of the kinetics are due to the $\sigma_{P_{700}PhQ}$ fraction, as predicted. The tail of decay elicited by the first actinic pulse in the closed fraction (i.e., $\sigma_{P_{700}^+PhQ^-}$; Fig. S4D, grey dashed line) has a much stronger contribution in the PsaA-F689N mutant, due to the slower oxidation of PhQ_A^-. This fraction and the $\sigma_{P_{700}PhQ}$ fraction (dashed blue line) together account for nearly all of the decay at 395 nm in the µs timescale in the mutant. Thus, nearly all of the decay at 395 nm in the $\sigma_{P_{700}PhQ^-}$ fraction (dash-dotted magenta line)

occurs in <100 ns and can be attributed to oxidation of PhQ_B^-. Therefore, within the confidence margin of the fits, it can be concluded that charge separation is biased towards ETC_B with a yield close to unity when PhQ_A^- is present in the system.

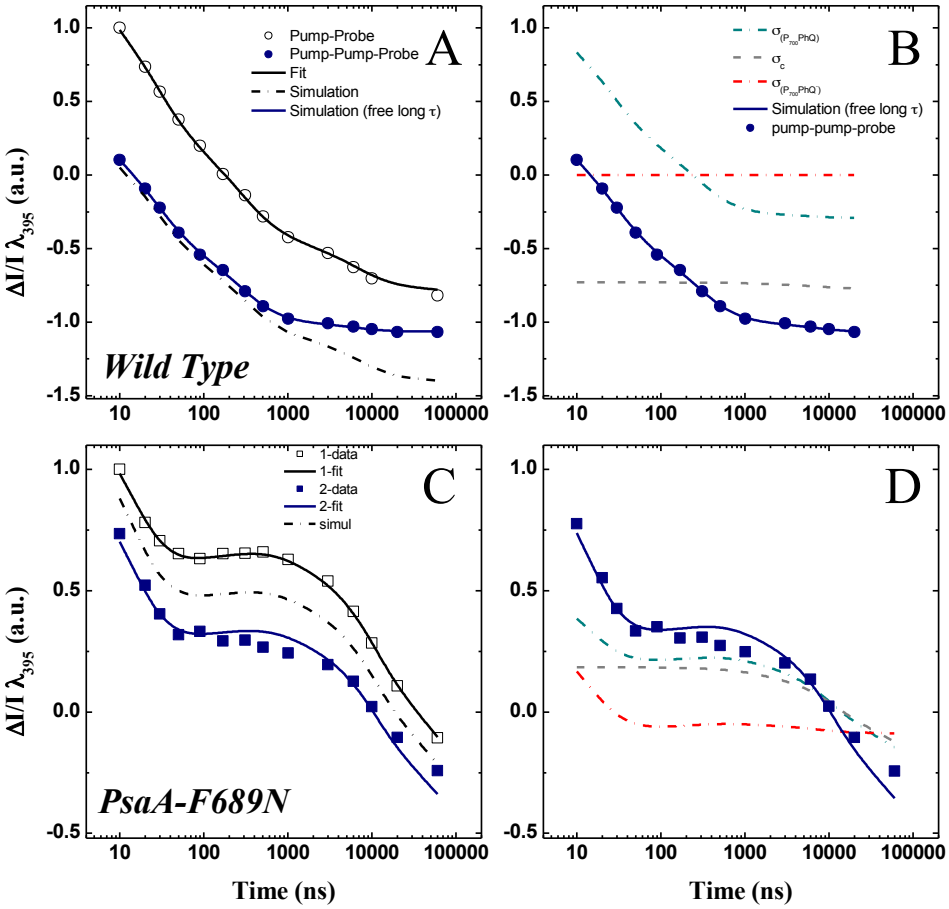

Figure S4. Comparison of experimental results and simulation of pump-pump-probe kinetics in the wild type (**A, B:** blue circles) and the PsaA-F689N strain (**C, D:** blue squares), monitored at 395 nm using $\Delta T = 15$ µs. The simulations are based on the fit of the pump-probe data, which are also shown for the WT (**A:** open circles) and the PsaA-F689N (**C:** open squares). The simulations according to Equation S3 are shown as black dash-dotted lines. The solid blue lines represent a mixed fit-simulation in which only the offset ($A_\infty(\lambda)$) is allowed to vary (PsaA-F689N) or the offset and the relative amplitudes of P_{700}^+ reduction (wild-type). Panels **B** and **D** show the de-convolution of the contributions to the pump-pump-probe absorption difference, for the case of WT (**B**) and the PsaA-F689N mutant (**D**) strains. Shown are the contributions of the signal arising from the different fractions after the second pump pulse: $\sigma_{P_{700}PhQ^-}$ (dash-dotted red line); $\sigma_{P_{700}PhQ}$ (dash-dotted green line); σ_{closed} (dashed grey line).

To further test this model, we have simulated the signal dependence as a function of the pump-pump delay time (Fig. S5), where the parameters related to the signal amplitude and the contribution of the "fast phase" have been calculated as for the experimental results. Both parameters are simulated satisfactorily. The fit to the simulations in terms of the exponential decays yields values τ_A=15 µs and τ_B=12 µs (7 µs and 55 µs for a bi-exponential recovery) which are very close to that obtained from the measurements (Figure 4, main body).

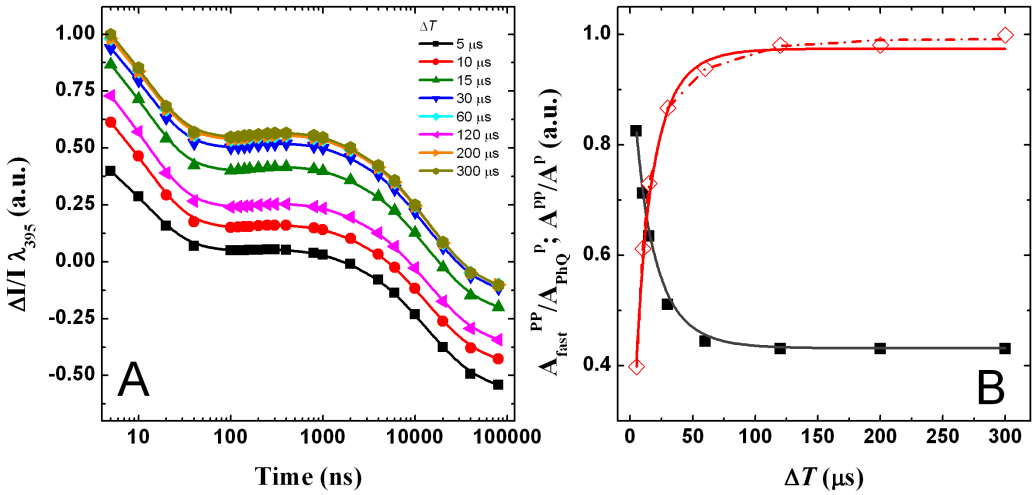

Figure S5. Panel A: Simulation of pump-pump-probe kinetics (at 395 nm) using different pump-pump delays (ΔT) ranging from 5 to 300 µs in the PsaA-F689N mutant strain. **Panel B:** Recovery of the difference absorption signal (A_0^{PP}/A_0^{P}) as a function of ΔT (red diamonds), and fractional contribution of the fast decay phase ($A_{fast}^{PP}=A_{40ns}^{PP} - A_0^{PP}$) to the difference absorption detected in the pump-pump-probe measurements (solid squares), calculated from the simulated kinetics shown in Panel **A**. The lines are fits to the estimated parameter using a single exponential (solid) or biexponential (dash-dotted) decay. The best fit for the initial amplitude recovery is obtained considering a biexponential relaxation ($\tau_{B,1}$= 7 µs and $\tau_{B,2}$=55 µs), whereas the decrease of the fractional amplitude of A_{fast}^{PP} as a function of ΔT is satisfactorily described by a single exponential (τ_A =15 µs).

It is thus possible to conclude that the presence of a meta-stable intermediate, such as PhQ_A^-, affects the primary photochemical process so that a *stable* charge separated state is formed only on ETC_B, resulting in reduction of PhQ_B. Hence, PSI essentially performs what could be considered a unidirectional (or extremely

asymmetric) ET as a result of the marked redistribution of the probability of utilization of the two active ET branches caused by the semiquinone anion in the A-branch.

Supporting References

1. Santabarbara, S., P. Heathcote, and M.C.W. Evans. 2005. Modelling of the electron transfer reactions in Photosystem I by electron tunnelling theory: the phylloquinones bound to the PsaA and the PsaB reaction centre subunits of PS I are almost isoenergetic to the iron–sulfur cluster F_X. Biochim. Biophys. Acta – Bioenergetics. 1708:283–310.

2. Santabarbara, S., L. Galuppini, and A.P. Casazza. 2010. Bidirectional electron transfer in the reaction centre of photosystem I. J. Integr. Plant. Biol. 52: 735–749.

3. Marcus, R.A., and N. Sutin 1985. Electron transfer in chemistry and biology. Biochim. Biophys. Acta. 811:265–322.

4. Hopfield, J.J. 1974. Electron transfer between biological molecules by thermally activated tunnelling. Proc. Natl. Acad. Sci. USA. 71:3640–3644.

5. Devault, D. 1980. Quantum mechanical tunnelling in biological systems. Cambridge University Press.

6. Jortner, J. 1976. Temperature Dependent Activation Energy for Electron Transfer Between Biological Molecules. J. Chem. Phys. 64:4860–4868.

7. Moser, C.C., and P.L. Dutton. 1992. Engineering protein structure for electron transfer function in photosynthetic reaction centers. Biochim. Biophys. Acta. 1101:171–176.

8. Page, C.C., C.C. Moser, X. Chen, and P.L. Dutton. 1999. Natural engineering principles of electron tunnelling in biological oxidation-reduction. Nature. 402:47–52

9. Jordan, P., P. Fromme, H.T. Witt, O. Klukas, W. Saenger, and Krauss N (2001) Three dimensional structure of cyanobacterial Photosystem I at 2.5 Å resolution. Nature. 411:909–917.

10. Agalarov R. and K. Brettel. 2003. Temperature dependence of biphasic forward electron transfer from the phylloquinone(s) A_1 in photosystem I: only the slower phase is activated. Biochim. Biophys. Acta – Bioenergetics. 1604:7–12.

11. Schlodder, E., K. Falkenberg, M Gergeleit, and K. Brettel. 1998. Temperature dependence of forward and reverse electron transfer from A_1^-, the reduced secondary electron acceptor in photosystem I. Biochemistry. 37:9466–9476

12. Santabarbara, S., K.E. Redding, and F. Rappaport. 2009. Temperature dependence of the reduction of P_{700}^+ by tightly bound plastocyanin in vivo. Biochemistry. 48:10457–10466.

13. Ali, K., S. Santabarbara, P. Heathcote, M.C.W. Evans, and S. Purton. 2006. Bidirectional electron transfer in photosystem I: replacement of the symmetry–breaking tryptophan close to the PsaB–bound phylloquinone A_{1B} with a glycine residue alters the redox properties of A_{1B} and blocks forward electron transfer at cryogenic temperatures. Biochim. Biophys. Acta – Bioenergetics. 1757:1623–1633.

14. Santabarbara, S., K. Reifschneider, A. Jasaitis, F. Gu, G. Agostini, D. Carbonera, F. Rappaport, and K.E. Redding. 2010. Interquinone electron transfer in photosystem I as evidenced by altering the hydrogen bond strength to the phylloquinone(s). J. Phys. Chem. B. 114:9300–9312.

15. Mula, S., M.D. McConnell, A Ching, N. Zhao N, H.L. Gordon, G. Hastings, K.E. Redding, and A. van der Est. 2012. Introduction of a hydrogen bond between phylloquinone PhQ_A and a threonine side-chain OH group in photosystem I. J. Phys. Chem. B. 116:14008–14016.

16. Brettel, K. 1997. Electron transfer and arrangement of the redox cofactor in photosystem I. Biochim. Biophys. Acta – Bionergetics. 1318:322–373.

17. Vos, M.H. and H.J. van Gorkom. 1988. Thermodynamics of electron transfer in Photosystem I studied by electric field-stimulated charge recombination. Biochim. Biophys. Acta – Bioenergetics. 934:293–302.

18. Byrdin, M., S. Santabarbara, F. Gu, W.V. Fairclough, P. Heathcote, K.E. Redding and F. Rappaport. 2006. Assignment of a kinetic component to electron transfer between iron-sulfur clusters F_X and $F_{A/B}$ of Photosystem I. Biochim. Biophys. Acta – Bioenergetics. 1757:1529–1538.

19. Müller, M.G., J. Niklas, W. Lubitz, and A.R. Holzwarth. 2003. Ultrafast transient absorption studies on Photosystem I reaction centers from Chlamydomonas reinhardtii. 1. A new interpretation of the energy trapping and early electron transfer stePSIn Photosystem I. Biophys. J. 85:3899–3922.

20. Müller, M.G., C. Slavov, R. Luthra, K.E. Redding, and A.R. Holzwarth. 2010. Independent initiation of primary electron transfer in the two branches of the photosystem I reaction center. Proc. Natl. Acad. Sci. USA. 107:4123–4128.

21. Li, Y., A. van der Est, M.G. Lucas, V.M. Ramesh, F. Gu, A. Petrenko, S. Lin, A.N. Webber, F Rappaport, and K.E. Redding. 2006. Directing electron transfer within Photosystem I by breaking H-bonds in the cofactor branches. Proc. Natl. Acad. Sci. USA. 103:2144–2149.

22. Giera, W., V.M. Ramesh, A.N. Webber AN, I. van Stokkum I, R. van Grondelle, and K. Gibasiewicz. 2010. Effect of the P_{700} pre-oxidation and point mutations near A_0 on the reversibility of the primary charge separation in Photosystem I from Chlamydomonas reinhardtii. Biochim. Biophys. Acta. – Bioenergetics. 1797:106–112.

23. McConnell, M., J.B. Cowgill, P.L. Baker, F. Rappaport and K.E. Redding. 2011. Double reduction of plastoquinone to plastoquinol in photosystem 1, Biochemistry, 50:11034–11046.

24. Lefebvre-Legendre, L., F. Rappaport, G. Finazzi, M. Ceol, C. Grivet, G. Hopfgartner, and J.D. Rochaix. 2007. Loss of phylloquinone in Chlamydomonas affects plastoquinone pool size and photosystem II synthesis, J Biol Chem, 282: 13250-13263.

25. Hervás, M., J.A. Navarro, and M.A. De La Rosa. 2003. Electron transfer between membrane complexes and soluble proteins in photosynthesis. Acc. Chem. Res. 36:798 – 805.

26. Hope, A.B. 2000. Electron transfers amongst cytochrome f, plastocyanin and photosystem I: kinetics and mechanisms. Biochim. Biophys. Acta–Bioenergetics. 1456:5–26.